IEEE Access
Multidisciplinary | Rapid Review | Open Access Journal

Received April 20, 2020, accepted May 6, 2020, date of publication May 11, 2020, date of current version June 1, 2020.

Digital Object Identifier 10.1109/ACCESS.2020.2993689

The Effect of PVP Concentration on Particle Size, Morphological and Optical Properties of Cassiterite Nanoparticles

NAIF MOHAMMED AL-HADA[1,2,3], ABBAS M. AL-GHAILI[4], HAIROLADENAN KASIM[5], MUNEER AZIZ SALEH[2], MOAYAD HUSEIN FLAIFEL[6,7], HALIMAH MOHAMED KAMARI[8], HUSSEIN BAQIAH[1], JIAN LIU[1], AND WANG JIHUA[1]

[1]Shandong Key Laboratory of Biophysics, Institute of Biophysics, Dezhou University, Dezhou 253023, China
[2]Nuclear Engineering Programme, School of Chemical and Energy Engineering, Universiti Teknologi Malaysia, Johore Bahru 81310, Malaysia
[3]Department of Physics, Faculty of Applied Science, Thamar University, Dhamar 87246, Yemen
[4]Institute of Informatics and Computing in Energy (IICE), Universiti Tenaga Nasional (UNITEN), Kajang 43000, Malaysia
[5]College of Computing and Informatics (CCI), Universiti Tenaga Nasional (UNITEN), Kajang 43000, Malaysia
[6]Department of Physics, College of Science, Imam Abdulrahman Bin Faisal University, Dammam 31441, Saudi Arabia
[7]Basic and Applied Scientific Research Center, College of Science, Imam Abdulrahman Bin Faisal University, Dammam 31441, Saudi Arabia
[8]Department of Physics, Faculty of Science, Universiti Putra Malaysia, Serdang 43400, Malaysia

Corresponding authors: Naif Mohammed Al-Hada (naifalhada@yahoo.com), Abbas M. Al-Ghaili (abbasghaili@yahoo.com; abbas@uniten.edu.my), Hairoladenan Kasim (hairol@uniten.edu.my), and Wang Jihua (jhw25336@126.com)

This work was supported in part by the Research Foundation for Advanced Talents of Dezhou University, in part by the Ministry of Higher Education Malaysia under Grant Q.J090000.21A4.00D20, in part by Universiti Teknologi Malaysia (UTM) under Grant FRGS/1/2013/SG06/UPNM/03/1, and in part by the Universiti Tenaga Nasional with Fund: Internal Research Grant Opex under Grant RJO10517919/iRMC/Publication.

ABSTRACT Different concentrations of polyvinylpyrrolidone (PVP) have been successfully employed to prepare high purity tetragonal cassiterite nanoparticles, and control the growth of particle size. The effect of PVP on the structural, morphological, size, composition, and optical properties of the prepared cassiterite nanoparticles has been investigated. It has been found that various characteristics of tetragonal cassiterite nanoparticles could be optimized by simply changing the values of PVP. The pure tetragonal cassiterite nanoparticles have been produced at the optimum calcination temperature. The XRD and SEM results indicated the structural and morphological properties of the tetragonal cassiterite nanoparticles, respectively. The particles' size and their distribution have been displayed by TEM images. The composition phase and the surface composition of the prepared samples have been evaluated via FTIR and XPS, respectively. The optical properties of the prepared tetragonal cassiterite nanoparticles have been studied using UV-vis and PL spectroscopy. Outcomes cassiterite nanoparticles are useful for antibacterial activity and application of solar energy.

INDEX TERMS Cassiterite nanoparticles, polyvinylpyrrolidone, thermal treatment technique, energy applications.

I. INTRODUCTION

Recently, a combination of organic and inorganic materials has been employed to produce a nanomaterials product and enhance its properties. The process of generating these improved products entails either a combination of artificial polymers and inorganic materials or blending converted nanoparticles (NPs) to polymer matrices. Due to their belonging to the nanomaterials, the first option could be most suitable for a new organisation of items. Progressive qualities were displayed by the new materials, predominantly, when they are organized with their microparticle equivalents [1], [2]. Therefore, nanomaterials have significant scientific and technological value. They include metal oxide nanoparticles, being a result of the nanoscale size as well as the increased amount of surface atoms because of the excellent physical and chemical characteristics [3]. By the increased surface to volume ratio and the quantum

The associate editor coordinating the review of this manuscript and approving it for publication was Ye Zhou.

confinement effect, their description is dependent upon them. An extent across almost every cultivation, as well as the field of human adventure, were utilized for their potential. A polymer chain is used as the setting for nanoparticle enhancement, as it synergistically integrates with the characteristics of the host polymer chain and the discrete nanostructures [4].

In reality, significant emphasis and a focal point were planned well by the nanoparticles that describe metal oxides rigid inside polymer matrices. Their physicochemical description from the outcome of the nanometre proportions of the particles differs dramatically from the one in bulk counterpart materials [5]. Fascinating magnetic, electrical, mechanical catalytic, and optical characteristics are said to be demonstrated by this sort of compound materials [6], [7]. The fabrication of metal-polymer or metal oxide semiconductor-polymer nanocomposites requires a broad range of approaches [8], [9]. One of these metal oxide semiconductors at the nanoscale, II-VI materials semiconductor comprised of tin II and oxygen VI as of the periodic table of obviously taking place elements is cassiterite [10]. The II-VI semiconductor cassiterite has a tetragonal crystalline structure and is believed to be a material with several benefits, and it displays a variety of captivating chemical and physical descriptions. cassiterite is an n-type materials transition semiconductor that involves narrow direct band gaps of 3.20 eV – 3.95 eV [11]–[13]. The matchless organisation produced an assortment of intriguing descriptions, indicating that applying the cassiterite nanomaterials to a diverse range of physical applications could be beneficial [14]–[16]. Primarily, it is helpful in optoelectronic devices similar to solar cells within their superior near pellucidum via the noticeable area of solar range [16]–[18]. Typically, this type of material is applied to areas including gas sensors, clear electrodes, and diodes [19]–[24]. An outcome of their fascinating features and different benefits (for instance, hierarchical SnO_2 Nanostructures [25], flower-like SnO_2 nanostructures [26]–[28], One-dimensional [29], Nanosheet-assembled hierarchical [30] and 1D and surface-functionalized SnO_2 nanosized of numerous structures [31]), was that a variety of SnO_2 nanomaterials were generated through diverse procedures. These procedures include, but are not limited to, the hydrothermal method [32]–[35], the carbothermal reduction [36], the thermal evaporation [37], [38], the microwave-assisted [39], the nano casting route [40], and the spray pyrolysis technique [41]. Nevertheless, the effectiveness of every technique for distributing nanosized materials is limited via re-accretion of separate nanostructures and the growth of an equipoise setting in induced circumstances, that dictates the measurement planes of the agglomerate of distributed nanosized. There are further limits surrounding temperature as well as the low level of the tolerance of several structures of metal or metal oxide semiconductor nanomaterials to motorized pressures. Those metal or semiconductor nanomaterials which involve a polymer chain are radically more dependable and consistent in the face of enlargement because of the enormous plummeting in their surface emission, mainly in comparison with plain particles. Through generating the metal oxide semiconductor nanoparticles (using any of the aforementioned techniques) and distributing the particles, an organic liquid such as a polymer could be utilized.

The polymer chain increases the synergy of the nanoparticles within it, thereby decreasing the energy necessary for their distribution. In terms of managing the allocation of nanoparticles, the polymer's role is key, in the face of growth as well as dissolving agents, the supplementary rule over the distributions of different employments are offered a helpful supply.

At the present research, cassiterite nanoparticles suchas the different structural shape of the acquired nanoparticles has been emphasized through the utility of calcined as well as PVP manufacturing, involving the device of those nanoparticles that can demonstrate multidimensional roles. The polymer has a vital position as it is a capping that potentially plays an important role in the development of the sample product. Consequently, knowing that the polymer controls the formation of the nanoparticles through the utility of its concentration is essential, as it diminishes the velocity of enlargement, improves the crystallinity, and promotes constancy and standardization inside the meaning of nanoparticles.

In this research study, cassiterite nanoparticles will be purely produced, and its related technique will be explained. This technique consists of the following two processes: (1) combining tin (II) chloride liquid dehydration, and (2) conducting a PVP capping agent process. Subsequently, a calcination process will be applied to the solution. Next, the morphology, structure, and optical properties will be investigated. This technique was selected due to its simplicity and the reasonability of its raw materials in comparison to other processes. The method discussed in this research study could be of interest to further advanced operations that contribute to many related fields [42]–[45].

II. EXPERIMENTAL WORK

A. MATERIALS

Tin (II) chloride dihydrate reagent, polyvinylpyrrolidone (PVP), and deionized waters' chemicals have been employed to prepare the cassiterite nanoparticles. A capping agent PVP and a metal precursor $SnCl_2.2H_2O$ (in which MW equals 29,000 and 225.65 g/mol respectively) have been used. They have been obtained from Sigma Aldrich and Acros Organics. All utilized chemicals included were offered. In addition, it suffered no further purification.

B. SAMPLES PREPARATION

Prior to the polymer solution incorporating 0.2 mmol of the tin (II) chloride dihydrate $SnCl_2{\cdot}2H_2O$ (MW is 225.65 g/mol), 100 ml of deionized ion was utilised to dissolve a range of PVP concentrations (0, 3, 4, 5 and 6 g). Acquiring a homogeneity solution required the composite

solution to be stirred for 2 hours. To eliminate the water, it had been poured onto a glass plate and heated to 80°C in the oven for one day. The resultant solid material had been fragmented down to powder, which entailed 15 minutes of labour within a grout and a grinder. The combination at that point experienced calcination at a temperature of 700°C for 180 minutes to obtain the pure cassiterite samples [46].

C. CHARACTERIZATION

A range of characterization procedures was applied to investigate the generated cassiterite nanoparticles features. Evaluating the structure required the utilisation of X-ray diffraction (XRD). The morphology, as well as the steadiness of the samples, had been examined using scanning electron microscopy (SEM). The morphology, i.e. the shape and dimensions of the particle, distribution of the particle dimension, and nanoparticles consistency, were recognized through the transmission electron microscopy. The FTIR spectrometer (Perkin Elmer model 1650) has been used to observe infrared spectra (ranging between 280 and 4000 cm^{-1}) standards, to verify the capping agents' abolition as well as inspecting the cassiterite residuals' inorganic composite after calcination, it required a pure product. Furthermore, a UV–vis spectrophotometer within photoluminescence (PL) were used to examine the optical features of samples at ambient temperatures, ranging between 200 and 800 nm.

III. RESULTS AND DISCUSSION

A. CALCINATION TEMPERATURE IMPACT ON PREPARED PRODUCT PROPERTIES

A summary of the previous work [46] is briefly outlined in this section of the report. The previous study conducted by the calcination temperature's initial impact on structural, morphology, and phase composition, as well as the optical properties of cassiterite (SnO_2) nanoparticles. The particle sizes of cassiterite nanoparticles have been increased to ∼4, 6, 9, and 15 nm uncertainty when the precursor of the cassiterite nanoparticles calcined at 500, 600, 700 and 800°C correspondingly (results of TEM and XRD). The crystallization point was examined from 500°C onwards. The total lack of natural absorption band acknowledged it through the FT-IR spectrum. The decline in the bandgap of the cassiterite nanoparticles was due to the increase in temperature as shown by the optical examinations. It is suggested that the decline in bandgap could be due to transitions between Sn^{2+} ion d-shell electrons' valance and conduction bands. The suitable calcination temperature of cassiterite nanoparticles had been examined at 700°C; by way of the temperature, this was determined to be the lowest temperature at which the nanoparticles retained their purity. Also, the least particle sizes and an approximately constant distributed of shape were investigated by the cassiterite nanoparticles, at this temperature.

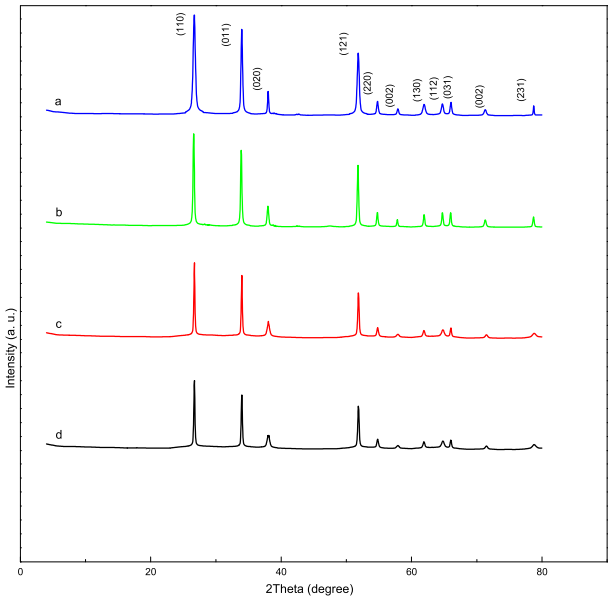

FIGURE 1. XRD results of the prepared cassiterite samples at the various amounts of PVP at (a) 3 (b) 4, (c) 5, and (d) 6 g.

B. PVP CONCENTRATION IMPACT ON THE PROPERTIES OF THE PRODUCT

1) ANALYSIS OF STRUCTURE

In order to ascertain the role of PVP, cassiterite products related XRD peaks at different concentrations of PVP (ranging between 0 and 6 g) and calcined at 700°C temperature have been investigated.

Characteristic XRD patterns are displayed in Figure 1. A sample with 3 g PVP is shown in Figure 1(a), which calcined at 700°C. A sharper, narrower diffraction peak demonstrating a crystalline cassiterite nanoparticles structure was formed. The cassiterite samples have a distinctive tetragonal crystalline structure (referring to the JCPDS 00-041-1445) [46]. The characteristic cassiterite nanoparticles XRD patterns once formed within 4 g and above of PVP at 700°C calcination are presented in Figure 1(b-d). The sharper and narrower diffraction peaks were shown by the spectrum, a crystalline cassiterite nanoparticles structure that has been formed was signified. Also, eminent values of PVP were recorded at the least crystallinity of the cassiterite products through declining the intensity of the peaks.

Within the TEM outcome, the diminishing of the crystalline limited the crystallinity enhancement, along with the growth of PVP at high ranges. The smallest crystallite size, along with the incline of PVP at high values are observed, as shown in table 1. The presence of peaks of numerous diffraction (110), (011), (020), (121), (220), (002), (130), (112), (031), (022) and (231) contained by patterns of diffraction indicates that the cassiterite nanoparticles samples have a representative tetragonal crystalline structure (JCPDS 00-041-1445) [59], [60].

The highest cassiterite nanoparticles peak can be attributed to the (110) index plane at $2\theta = 26.8°$. The maximum severe

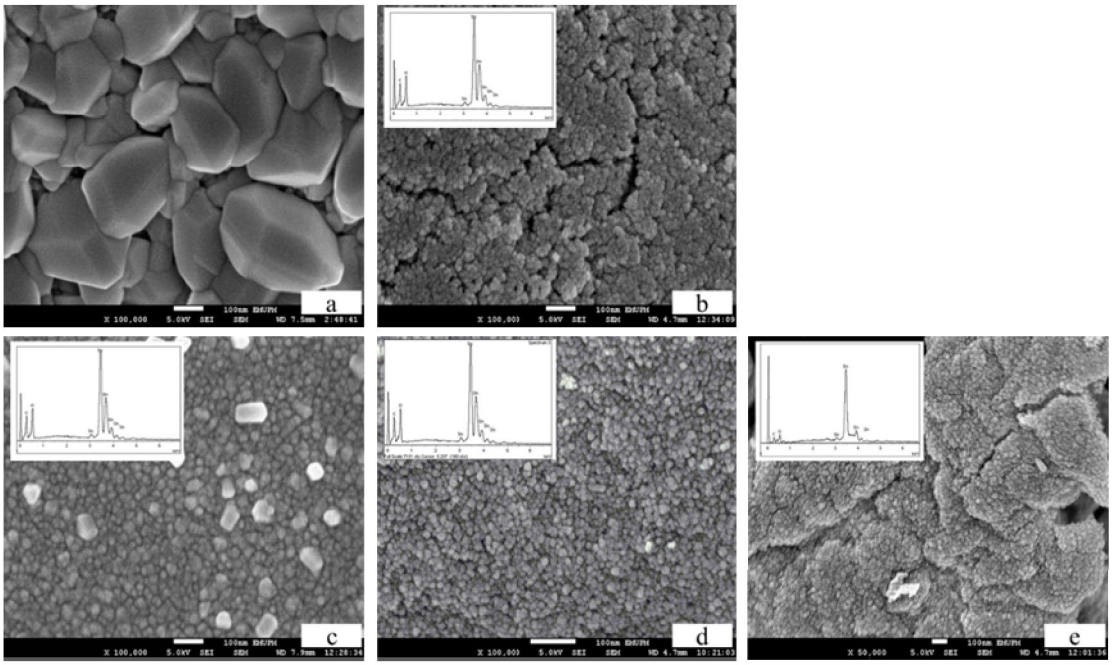

FIGURE 2. SEM images of the prepared cassiterite samples at various amount of PVP at (a) 0 (b) 3, (c) 4, (d) 5 and (e) 6 g.

TABLE 1. XRD, TEM and bandgap results for the cassiterite nanoparticles at various PVP.

cassiterite samples	PVP Concentration (g)	Crystallite size (nm)	Particle size (nm)	Eg (eV)
cassiterite 1	0	-	-	3.33
cassiterite 2	3	18	19±3	3.62
cassiterite 3	4	8	9±2	3.80
cassiterite 4	5	6	7±3	3.86
cassiterite 5	6	5	5±2	3.91

peak (110)'s extension recognized the cassiterite nanoparticles regular crystallite dimension, through the employment of the extremely observed Debye-Scherrer equation. The equation is as follows:

$$D = 0.9\lambda/\beta \cos\theta$$

where D is size of crystallite (nm), β is full width of diffraction line size at a half of the highest intensity which is intended in radians. λ is the X-ray wavelength of Cu Kα = 0.154 nm, and θ is the Bragg's angle [47]. The crystallite sizes of cassiterite nanoparticles were examined to distance from 22 nm to 3 nm, along with an expanding PVP concentration (from 3 to 6 g).

2) SEM ANALYSIS

The purpose of using SEM was to aid in the examination of the cassiterite nanoparticles' surface, with and without PVP, as depicted in Figure 2. A heat-based treatment method was employed. The cassiterite nanoparticles fabrication at 700°C temperatures without PVP is shown in Figure 2(a). The structures were displayed to be crudely solely consistently dispersed and crystal in shape and oblique crystal procedure [48]. A PVP concentration extending from 3 to 6 g within an amalgamation assembled the SEM recordings of cassiterite nanoparticles was demonstrated in Figure 2(b-e). Moderately nano-porous and moderately nanospheres' shapes [2], [49] form the morphology, as displayed in the outcomes. A composite with some nanospheres shapes is represented in Figure 2(b-c). According to Figure 2(c-e), the quantity of nanospheres forms creates a pact with growth inside the PVP concentration. As shown in Figure 2(e), there is a correlation between stable PVP concentration growth and the cassiterite nanoparticles forms roughly converted into small nanospheres forms. In other words, the PVP capping typically occurs more with any increase of its quantity. Consequently, when PVP increases, the grain size of the product becomes smaller because of PVP capping occurrence. The aggregation at low PVP quantity tends to form a larger grain size; and vice versa, the aggregation at higher PVP quantity tends to make uniform shape, near-spherical grain with regularities and smaller nanoparticles as shown in figure 2(d-e) [50].

3) TEM ANALYSIS

The cassiterite nanoparticles product that was prepared within a water-based liquid (incorporating metal precursor and the diverse values of PVP's range, i.e. 0, 3, 4, 5 and 6 g) as a capping agent, for particles stabilized in line with decreasing the enlargements' growth have been investigated using TEM. The cassiterite nanoparticles samples that were steady without PVP are depicted in Figure 3(a), through the utility of a heat-based treatment procedure, at 700°C. Forming the

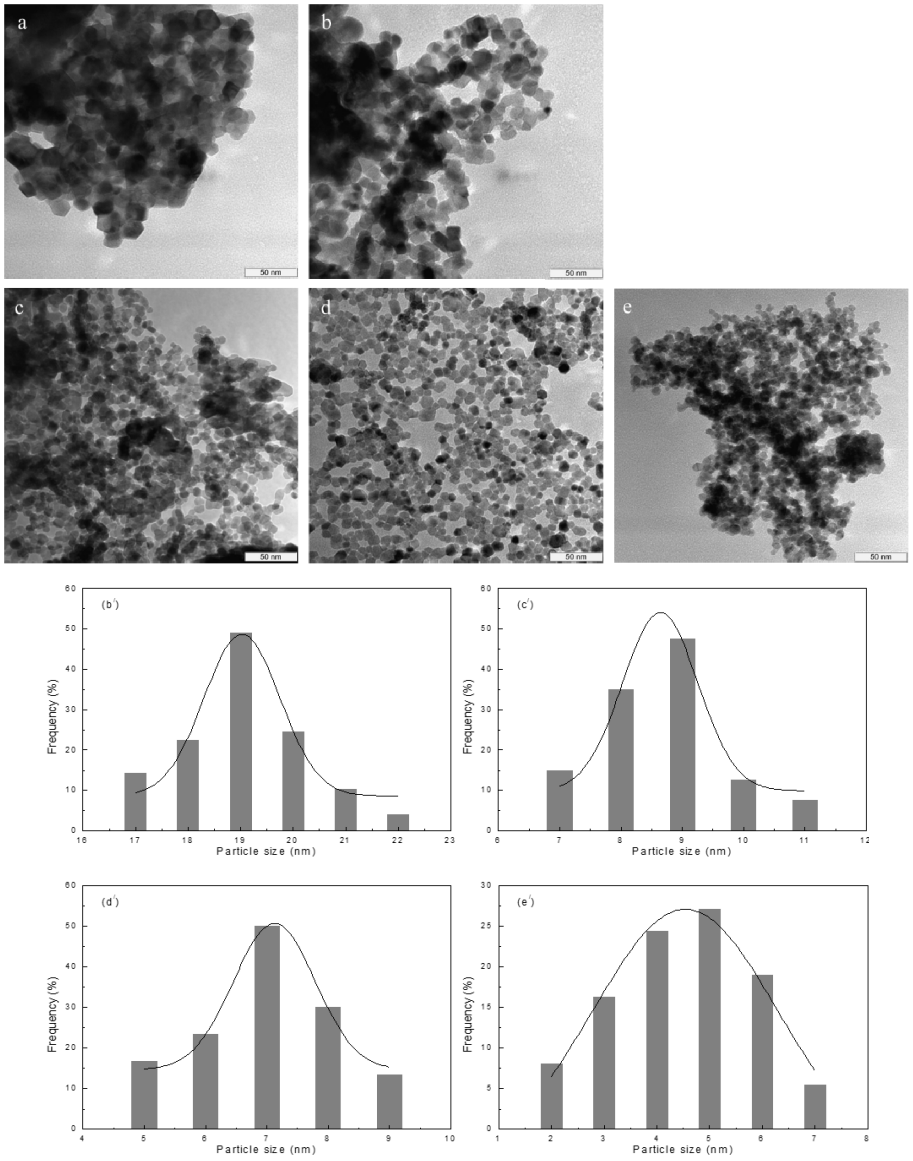

FIGURE 3. TEM images and particle size distribution of the prepared cassiterite samples at various amount of PVP at (a) 0 (b, b/) 3, (c, c/) 4, (d, d/) 5 and (e, e/) 6 g.

cassiterite nanoparticles did not require any assistance from PVP. Yet, in the surroundings, it had been observed that the products required a homogenous distribution of form and were unequally accrued in several places.

In common means, none of the methods or procedures necessitated distributing. Consequently, it is ascertained that a lack of PVP in the nanoparticles' generation will mean that the lesser particles accrue and ultimately convert into well-built ones, which is an important outcome for surface energy. Moreover, the figure aimed at several areas recorded melting uniform morphology as well as an opacity as to particle dimension dispersion, which is due to the employment of PVP. The characteristic particle dimension at a calcination temperature of 700°C is complicated to examine through the use of just ImageJ or other software.

The TEM images for particle dimension and particle dimension distribution in cassiterite nanoparticles samples that were made ready within PVP at concentrations 3, 4, 5, and 6 g and calcined 700°C are displayed in Figure 3(b-e). The homogenous morphology and even particle size dispersion were shown as a sign of the findings. The typical particle size at different PVP concentrations increasing from 3 to 6 g is about 22 $\pm$ 2 nm to 3 $\pm$ 4 nm correspondingly. These outcomes are almost in accordance with the findings of the XRD results. The particle shape is spherical and elliptical, comparable to those recorded in earlier reports [2]. The results also propose that the size of noted particle is smaller, which is in line with the rising PVP amount. This could be explained that as the PVP increases, the bigger particles became constrained (or capped) within the development with

enlargement slowed to generate smaller particles. Furthermore, the results show that the recorded particle size got smaller, in accordance with an increment in amount of PVP concentration. This can be explained by the fact that, as the PVP got stronger, the bigger particles became restricted (or capped) and expansion and accretion was slowed to produce the particles. Also, the restriction of growth and the decrease of accumulation in samples with PVP lead to cap particles, as long as the PVP concentration is high enough. If contrasted with the concentration of PVP when it was boosted to 3 g, it is clear to see that the sample nanoparticles formed had a typical dimension of 22 ± 2 nm. They gradually became more homogenous in form and more than in conditions without PVP as shown in Figure 3(b). Nevertheless, because of the still equally minor concentration of PVP, the nanoparticles grew anyway – when capping them and confining their growth, there was no sufficient PVP. It was complex to build up the cassiterite nanoparticles and they were approximately homogenous in shape when the PVP amount was raised to 5 g, as depicted in Figure 3(c-e). However, in these circumstances, dimensions from 15 to 4 nm were the extent for the cassiterite nanoparticles (refer to Table 1). Identical results were observed with the use of PVP amounts of 4, 5 and 6 g.

When generated cassiterite nanoparticles within PVP, a minor stage of growth with the particles and a larger standardized shape is displayed by the TEM findings of the developed cassiterite nanoparticles, as a procedure of capping and restraint throughout the development. The heat-based treatment method also provides the advantages of generating cassiterite, such as an approximately homogenous alignment and particle size dispersal. For professional regulating the extension of the nanoparticles and lowering the rate of accretion, the inclusion of PVP could be beneficial [45], [50]–[58].

4) PHASE COMPOSITION

FTIR investigations were utilized to calculate the effect of the PVP amount when samples formed to cassiterite nanoparticles, devoid of the presence of any untreated trace agent. Through investigating the exchange between cassiterite nanoparticles products and PVP, it can also be recognized. The inorganic and organic components of samples with a PVP concentration spanning from 0 - 6 g over the wavenumber variety of 280-4000 cm-1 were shown in the spectra outcome in Figure 4. The solo peaks that can be clarified through the existence of cassiterite, in the nonexistence of PVP are verified by Figure 4(a). The solo peaks which could be clarified through cassiterite nanoparticles within the help of a PVP concentration are shown in Figure 4(b-e). With the cassiterite spectra values and the existence of single absorption peaks, this indicates that the cassiterite was formed via a heat-based treatment process. The accelerated crystallinity of the cassiterite nanoparticles could explain the subsistence of single absorption peaks and the recorded adjustment in the wavenumber for the cassiterite nanoparticles spectra values (in the existence of increasing PVP), which was attained through the conduction of heat-based treatment methods and

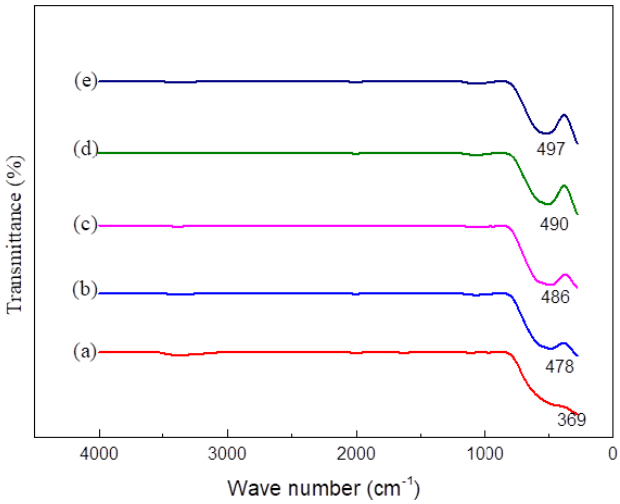

FIGURE 4. FTIR spectra of the prepared cassiterite 2 samples at various amount of PVP at (a) 0 (b) 3, (c) 4, (d) 5 and (e) 6 g.

PVP concentration. The 369, 478, 486, 490 and 497 cm^{-1} absorption peaks relate to the O–Sn–O vibration [46]. When the PVP concentration is less than 6 g, it is possible to attain cassiterite nanoparticles that have equivalent purity to those signified by the values presented in Figure 4(c). This denotes that the cassiterite nanoparticles were conquered through intense values of the organic materials [59], [60].

5) UV-VIS ANALYSIS

The impact of 700°C calcination on the optical properties of prepared cassiterite nanoparticles and the altering concentrations of PVP were processed and will be outlined in the next section. The energy band gap related result for every sample calcined at 700°C and altering amount of PVP were considered utilizing the reflectance spectra values and the Kubelka-Munk equation, which is as follows:

$$(F(R_\infty).hv)^2 = (A(hv - E_g))$$

where $F(R_\infty)$ is the Kubelka-Munk role or the so-known remission parameter; (hv) is the incident photon energy; A is a dependant on the evolution probability [59] and the diffuse reflectance (R_∞); (R_∞) is the diffuse reflectance which is collected from $R_\infty = R_{sample}/R_{standard}$ [60].

Figure 5 revealed the values of $(F(R_\infty).hv)^2$ versus (hv). Accomplishing the (hv) axis [61], [62] requires the direct line ranges on the diagram to be extended, in order for the model band gap values of cassiterite nanoparticles to be considered at a variety of PVP concentrations. The optical band gap was investigated, and it was found that it extended, together with mounting PVP concentrations, with an extent from 3.33 eV at 0 g to 3.91 eV at 6 g, which is presented in Figure 5. The decline in particle dimension and crystallinity rates elucidation were applied to clarify the extension in the energy bandgap within the increasing PVP, within being a sign by XRD values. It is believed that, when the particle dimension declines, the number of atoms required for manufacturing an

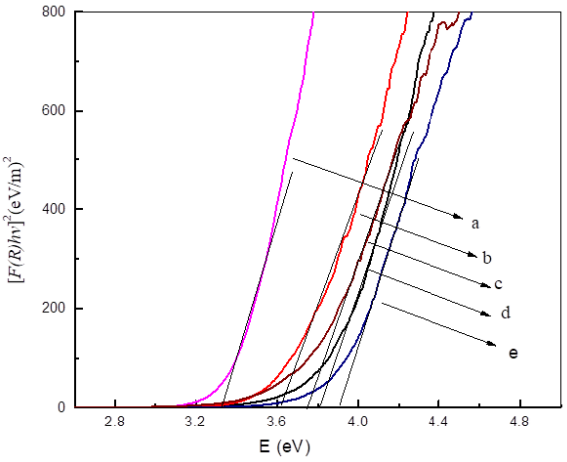

FIGURE 5. The energy band gap of the prepared cassiterite samples at the various amount of PVP at (a) 0 (b) 3, (c) 4, (d) 5 and (e) 6 g.

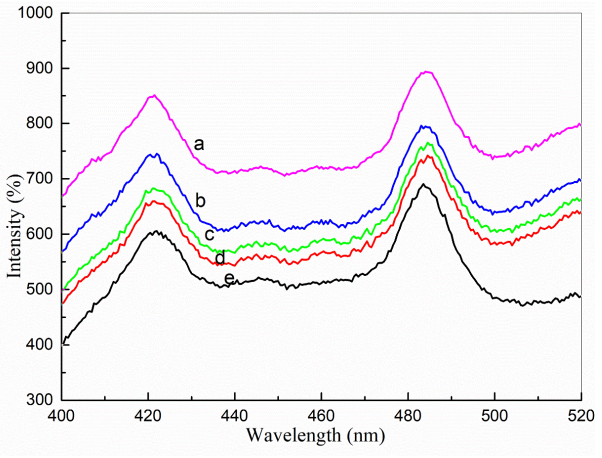

FIGURE 6. PL spectra of the prepared cassiterite samples at various amount of PVP at (a) 0 (b) 3, (c) 4, (d) 5 and (e) 6 g.

atom also drops and declines. Subsequently, this causes the valence and transmission electrons to decrease, which results in the particles' ion core becoming a more interesting and valuable focal point. The extension through the bandgap of the atoms is the ultimate outcome.

The energy band gaps were displayed to extend alongside an increase in PVP, as shown in Figure 5 (refer to Table 1). The altering concentrations of PVP were examined to allow the incline of the bandgap values of the cassiterite nanoparticles to be produced, and the observations are presented in Figure 5. This implies that the change in the bandgap values was due to the cassiterite particle dimension. The shifts between the partially hidden valence and transmission bands of the d-shell electrons of Sn^{2+} ions clarification can help to clarify the inclines in the bandgap.

The subdivision dimension collision on the bandgap should not be disregarded. Due to the declining particle dimensions, there is an altar in the band arrangement and inside the description of the matter. The bandgap values increased when the dimension of the nanoparticle's declines. Consequently, it was decided that the transmission band of s-electrons and p-electrons are protected when at inclined energy settings, however they are not in close immediacy to one another and their dimensions are comparatively compact. When in a direction besides the Fermi stage – which is approved to be extremely isolated from the middle of the atom – the nuclear perspective of the transmission electrons is major and declined all shifts, including legal quantum numbers, showing incorporation energy equivalent to the transfer band energy.

6) PL ANALYSIS

In this section, the energy levels in the cassiterite products' arrangement is examined with the help of the photoluminescence (PL) utility. Utilizing a spectrometer and plot peaks along spectra values replicates a straight result of energy levels for the sample to calculate the degree of luminescence. The nanometer-scale crystals can be tailored in composition (II−VI semiconductors), size, shape, and surface ligands, ensuring the ability to easily engineer properties including gap energy, self-assembly capability, photoluminescence efficiency, and quantum confinement effect. The samples were prepared within a heat-based calcination procedure and altering PVP concentrations. Figure 6 presents the PL spectra values of the cassiterite nanoparticles when they are within the excitation wavelength of 380 nm at room temperature.

The benefits of altering PVP concentrations under a 700°C supported PL spectra values formation of cassiterite nanoparticles were examined under ambient temperature at excitation of 390 nm. A broad-ranging emission is displayed by the PL spectra values of the cassiterite nanoparticles that were all set within concentration of PVP, within an extent from ∼425 nm to 487 nm, as shown in Figure 6. Ultimately, this is because of the 'composite' collision and the power states which survive between the valence and transmission bands. These tremendous plots consist of a pair of minor sub bands under ∼487 nm [46]. Electron-hole pairs within oxygen and Sn vacancies are correspondingly recombined [63]. Clarification can help to elucidate the first peak. The second peak can be explained by the distinct composites being recorded throughout the PL spectra values of the cassiterite nanoparticles product, which itself is attributable to the conversion that took place between the valence and the transmission bands [64].

The abovementioned peak at 487 nm is correlated to deep energy stages emission of cassiterite. Inherent defects cause it to manifest throughout the cassiterite nanoparticles. It will be clear for observing the regular PVP inclines that leads to slow intensity declines when several PVP concentrations are contrasted, on top of the minor particle dimensions. Investigations show that when the peak with the most amount is contrasted with minor intense spectral bands in PVP of fewer than 6 g, there is a robust tetragonal crystalline structure and only a minor amount of inner and surface defects.

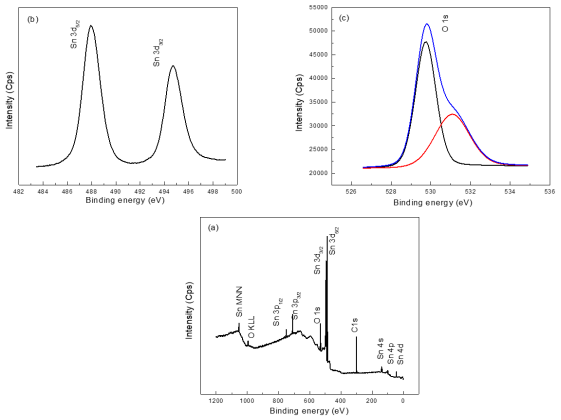

FIGURE 7. XPS spectra for survey (a), tin (b), and oxygen (c).

7) COMPOSITIONAL ANALYSIS

The X-ray photoelectron spectroscopy (XPS) was employed to examine the tin and oxygen elements' compositions phase and chemical state. Figure 7(a) presented the XPS outcomes that completed establishing the reality of Sn, O and C elements, while Figure 7(b) displayed the high-res XPS spectra for Sn $3d_{3/2}$ and Sn $3d_{5/2}$.The outcomes that were shown in earlier research [2], [65]–[67] were with the binding energies of 487.8 eV for Sn $3d_{5/2}$ peak and 494.9 eV for the Sn $3d_{3/2}$ peak. The binding energies of 529.7 eV and 531.1 eV for two forms of oxygen (Fig. 7c) were shown by the deconvoluted O 1s spectrum, which was seen to be related within cassiterite [68], [69]. These outcomes are evidence of the pure nature of oxidation states of the nanoparticle elements.

IV. CONCLUSION

This research summarizes the PVP function and its role through the production of cassiterite nanoparticles, and detailed the treatment process that was conducted. When summarized for the period of the examination of XRD outcomes, TEM results, and FTIR spectra outcomes, PVP consists of four necessary roles through the production of cassiterite nanoparticles. Firstly, it adjusts the extension nanoparticles nucleation that are dependent on the PVP concentration. Secondly, it restricts the accumulation of nanoparticles. Thirdly, it could enhance the degree of crystallinity in the nanoparticles. Finally, it eases particle enlargement with a homogenous dispersal of size and form.

The optimum amount utilized was determined to be 5 g, as this was the lowest level at which the particles maintained their high purity. Also, the least particle dimension and an approximately homogenous dispersal of form have been displayed by this concentrations' nanoparticles.

Some applications, such as solar cells or sensors, might employ this helpful product due to the numerous mixtures of PVP that could generate various sizes of cassiterite nanostructures that can cause various bandgaps values, and as such, could absorb several wavelengths of solar energy for a perfect solar cells' application.

REFERENCES

[1] X. Ding, S.-C.-S. Lin, B. Kiraly, H. Yue, S. Li, I.-K. Chiang, J. Shi, S. J. Benkovic, and T. J. Huang, "On-chip manipulation of single microparticles, cells, and organisms using surface acoustic waves," *Proc. Nat. Acad. Sci. USA*, vol. 109, no. 28, pp. 11105–11109, Jul. 2012.

[2] C.-L. Ma and X.-D. Sun, "Preparation and characterization of SnO_2 nanoparticles with a surfactant-mediated method," *Nanotechnol.*, vol. 13, no. 5, p. 565, 2002.

[3] X. W. Lou, D. Deng, J. Y. Lee, J. Feng, and L. A. Archer, "Self-supported formation of needlelike Co_3O_4 nanotubes and their application as lithium-ion battery electrodes," *Adv. Mater.*, vol. 20, no. 2, pp. 258–262, Jan. 2008.

[4] S. Nie, Y. Xing, G. J. Kim, and J. W. Simons, "Nanotechnology applications in cancer," *Annu. Rev. Biomed. Eng.*, vol. 9, pp. 257–288, Aug. 2007.

[5] T. Rodenas, "Metal-organic framework nanosheets in polymer composite materials for gas separation," *Nature Mater.*, vol. 14, no. 1, pp. 48–55, 2015.

[6] S. Komarneni, "Nanocomposites," *J. Mater. Chem.*, vol. 2, no. 12, pp. 1219–1230, 1992.

[7] C.-H. Lai, M.-Y. Lu, and L.-J. Chen, "Metal sulfide nanostructures: Synthesis, properties and applications in energy conversion and storage," *J. Mater. Chem.*, vol. 22, no. 1, pp. 19–30, 2012.

[8] N. M. Al-Hada, H. M. Kamari, M. A. Saleh, M. H. Flaifel, A. M. Al-Ghaili, H. Kasim, A. A. Baqer, E. Saion, and W. Jihua, "Morphological, structural and optical behaviour of PVA capped binary $(NiO)_{0.5}$ $(Cr_2O_3)_{0.5}$ nanoparticles produced via single step based thermal technique," *Results Phys.*, vol. 17, Jun. 2020, Art. no. 103059.

[9] H. Tecimer, S. O. Tan, and S. Altindal, "Frequency-dependent admittance analysis of the metal–semiconductor structure with an interlayer of Zn-doped organic polymer nanocomposites," *IEEE Trans. Electron Devices*, vol. 65, no. 1, pp. 231–236, Jan. 2018.

[10] M. Cardona and Y. Y. Peter, *Fundamentals of Semiconductors*. Berlin, Germany: Springer, 2005.

[11] Z. W. Pan, "Nanobelts of semiconducting oxides," *Science*, vol. 291, no. 5510, pp. 1947–1949, Mar. 2001.

[12] Z. Li, Y. Zhou, T. Yu, J. Liu, and Z. Zou, "Unique Zn-doped SnO_2 nanoechinus with excellent electron transport and light harvesting properties as photoanode materials for high performance dye-sensitized solar cell," *CrystEngComm*, vol. 14, no. 20, pp. 6462–6468, 2012.

[13] C. E. Benouis, M. Benhaliliba, Z. Mouffak, A. Avila-Garcia, A. Tiburcio-Silver, M. O. Lopez, R. R. Trujillo, and Y. S. Ocak, "The low resistive and transparent al-doped SnO_2 films: P-type conductivity, nanostructures and photoluminescence," *J. Alloys Compounds*, vol. 603, pp. 213–223, Aug. 2014.

[14] C. N. R. Rao, A. Müller, and A. K. Cheetham, *The Chemistry of Nanomaterials: Synthesis, Properties and Applications*. Hoboken, NJ, USA: Wiley, 2006.

[15] H. D. Beyene and T. G. Ambaye, "Application of sustainable nanocomposites for water purification process," in *Sustainable Polymer Composites and Nanocomposites*. Berlin, Germany: Springer, 2019, pp. 387–412, doi: 10.1007/978-3-030-05399-4_14.

[16] S. Sharma, S. P. Usha, A. M. Shrivastav, and B. D. Gupta, "A novel method of SPR based SnO_2: GNP nano-hybrid decorated optical fiber platform for hexachlorobenzene sensing," *Sens. Actuators B, Chem.*, vol. 246, pp. 927–936, Jul. 2017.

[17] I. Concina and A. Vomiero, "Metal oxide semiconductors for dye- and quantum-dot-sensitized solar cells," *Small*, vol. 11, no. 15, pp. 1744–1774, Apr. 2015.

[18] X. W. Lou, Y. Wang, C. Yuan, J. Y. Lee, and L. A. Archer, "Template-free synthesis of SnO_2 hollow nanostructures with high lithium storage capacity," *Adv. Mater.*, vol. 18, no. 17, pp. 2325–2329, Sep. 2006.

[19] J. S. Kim, Y. B. Kim, S. K. Baek, Y. D. Yun, S. H. Jung, S. W. Cho, C. H. Ahn, and H. K. Cho, "Compositionally graded SnO_2/TiO_2 bi-layered compounds with dramatically enhanced charge transport efficiency for self-driven water purification applications," *J. Alloys Compounds*, vol. 776, pp. 839–849, Mar. 2019.

[20] M. Tatariants, S. Yousef, M. Skapas, R. Juskenas, V. Makarevicius, S.-I. Lukošiūtė, and G. Denafas, "Industrial technology for mass production of SnO_2 nanoparticles and PbO_2 microcube/microcross structures from electronic waste," *J. Cleaner Prod.*, vol. 203, pp. 498–510, Dec. 2018.

[21] M. Maleki Shahraki, M. D. Chermahini, S. Alipour, P. Mahmoudi, I. Safaee, and M. Abdollahi, "Ultra-high voltage SnO_2 based varistors prepared at low temperature by two-step sintering," *J. Alloys Compounds*, vol. 805, pp. 794–801, Oct. 2019.

[22] T. Xin, F. Diao, C. Li, H. Feng, G. Liu, J. Zou, Y. Ding, B. Liu, and Y. Wang, "Synergistic effect of hierarchical SnO_2 nanorods/Fe_2O_3 hexahedrons with enhanced performance as lithium ion battery anodes," *Mater. Res. Bull.*, vol. 99, pp. 196–203, Mar. 2018.
[23] Y. Liu, Y. Jiao, Z. Zhang, F. Qu, A. Umar, and X. Wu, "Hierarchical SnO_2 nanostructures made of intermingled ultrathin nanosheets for environmental remediation, smart gas sensor, and supercapacitor applications," *ACS Appl. Mater. Interface*, vol. 6, no. 3, pp. 2174–2184, Feb. 2014.
[24] C. Wang, C. Shao, X. Zhang, and Y. Liu, "SnO_2 nanostructures-TiO_2 nanofibers heterostructures: Controlled fabrication and high photocatalytic properties," *Inorganic Chem.*, vol. 48, no. 15, pp. 7261–7268, 2009.
[25] H. Wang and A. L. Rogach, "Hierarchical SnO_2 nanostructures: Recent advances in design, synthesis, and applications," *Chem. Mater.*, vol. 26, no. 1, pp. 123–133, 2013.
[26] H. Wang, Q. Liang, W. Wang, Y. An, J. Li, and L. Guo, "Preparation of flower-like SnO_2 nanostructures and their applications in gas-sensing and lithium storage," *Crystal Growth Des.*, vol. 11, no. 7, pp. 2942–2947, 2011.
[27] J. Huang, K. Yu, C. Gu, M. Zhai, Y. Wu, M. Yang, and J. Liu, "Preparation of porous flower-shaped SnO_2 nanostructures and their gas-sensing property," *Sens. Actuators B, Chem.*, vol. 147, no. 2, pp. 467–474, Jun. 2010.
[28] K. Wongsaprom, A. Winyayong, and S. Maensiri, "Synthesis and room-temperature ferromagnetism in flower-like SnO2 nanostructures," *J. Phys., Conf. Ser.*, vol. 1144, Dec. 2018, Art. no. 012042.
[29] J. Pan, H. Shen, and S. Mathur, "One-dimensional SnO_2 nanostructures: Synthesis and applications," *J. Nanotechnol.*, vol. 2012, Sep. 2012, Art. no. 917320.
[30] T. Li, W. Zeng, H. Long, and Z. Wang, "Nanosheet-assembled hierarchical SnO_2 nanostructures for efficient gas-sensing applications," *Sens. Actuators B, Chem.*, vol. 231, pp. 120–128, Aug. 2016.
[31] V. Bonu, B. K. Sahu, A. Das, S. Amirthapandian, S. Dhara, and H. C. Barshilia, "Sub-wavelength waveguide properties of 1D and surface-functionalized SnO_2 nanostructures of various morphologies," *Beilstein J. Nanotechnol.*, vol. 10, no. 1, pp. 379–388, Feb. 2019.
[32] N. Talebian and F. Jafarinezhad, "Morphology-controlled synthesis of SnO_2 nanostructures using hydrothermal method and their photocatalytic applications," *Ceram. Int.*, vol. 39, no. 7, pp. 8311–8317, Sep. 2013.
[33] P. Sun, X. Mei, Y. Cai, J. Ma, Y. Sun, X. Liang, F. Liu, and G. Lu, "Synthesis and gas sensing properties of hierarchical SnO_2 nanostructures," *Sens. Actuators B, Chem.*, vol. 187, pp. 301–307, Oct. 2013, doi: 10.1016/j.snb.2012.11.043.
[34] P. Sun, X. Zhou, C. Wang, B. Wang, X. Xu, and G. Lu, "One-step synthesis and gas sensing properties of hierarchical Cd-doped SnO_2 nanostructures," *Sens. Actuators B, Chem.*, vol. 190, pp. 32–39, Jan. 2014, doi: 10.1016/j.snb.2013.08.045.
[35] A. Kar, J. Olszówka, S. Sain, S.-R.-I. Sloman, O. Montes, A. Fernández, S. K. Pradhan, and A. E. H. Wheatley, "Morphological effects on the photocatalytic properties of SnO_2 nanostructures," *J. Alloys Compounds*, vol. 810, Nov. 2019, Art. no. 151718, doi: 10.1016/j.jallcom.2019.151718.
[36] S. Sun, G. Meng, M. Zhang, X. An, G. Wu, and L. Zhang, "Synthesis of SnO_2 nanostructures by carbothermal reduction of SnO_2 powder," *J. Phys. D, Appl. Phys.*, vol. 37, no. 3, p. 409, 2004.
[37] H. W. Kim, N. H. Kim, J. H. Myung, and S. H. Shim, "Characteristics of SnO_2 fishbone-like nanostructures prepared by the thermal evaporation," *Phys. Status Solidi (A)*, vol. 202, no. 9, pp. 1758–1762, Jul. 2005.
[38] Y. Lingmin, F. Xinhui, Q. Lijun, M. Lihe, and Y. Wen, "Dependence of morphologies for SnO_2 nanostructures on their sensing property," *Appl. Surf. Sci.*, vol. 257, no. 7, pp. 3140–3144, Jan. 2011, doi: 10.1016/j.apsusc.2010.11.013.
[39] Q. Wang, C. Wang, H. Sun, P. Sun, Y. Wang, J. Lin, and G. Lu, "Microwave assisted synthesis of hierarchical Pd/SnO_2 nanostructures for CO gas sensor," *Sens. Actuators B, Chem.*, vol. 222, pp. 257–263, Jan. 2016.
[40] V. K. Tomer and S. Duhan, "A facile nanocasting synthesis of mesoporous Ag-doped SnO_2 nanostructures with enhanced humidity sensing performance," *Sens. Actuators B, Chem.*, vol. 223, pp. 750–760, Feb. 2016, doi: 10.1016/j.snb.2015.09.139.
[41] Anusha, B. Sudarshan Acharya, A. Antony, A. Ani, I. V. Kityk, J. Jedryka, P. Rakus, A. Wojciechowski, P. Poornesh, and S. D. Kulkarni, "Laser stimulated second and third harmonic optical effects in F: SnO_2 nanostructures grown via chemical synthetic route," *Opt. Laser Technol.*, vol. 119, Nov. 2019, Art. no. 105636, doi: 10.1016/j.optlastec.2019.105636.
[42] N. M. Al-Hada, E. B. Saion, A. H. Shaari, M. A. Kamarudin, M. H. Flaifel, S. H. Ahmad, and S. A. Gene, "A facile thermal-treatment route to synthesize ZnO nanosheets and effect of calcination temperature," *PLoS ONE*, vol. 9, no. 8, 2014, Art. no. e103134.
[43] N. M. Al-Hada, E. B. Saion, A. H. Shaari, M. A. Kamarudin, M. H. Flaifel, S. H. Ahmad, and A. Gene, "A facile thermal-treatment route to synthesize the semiconductor CdO nanoparticles and effect of calcination," *Mater. Sci. Semiconductor Process.*, vol. 26, pp. 460–466, Oct. 2014.
[44] N. M. Al-Hada, H. M. Kamari, A. H. Shaari, and E. Saion, "Fabrication and characterization of manganese–zinc ferrite nanoparticles produced utilizing heat treatment technique," *Results Phys.*, vol. 12, pp. 1821–1825, Mar. 2019, doi: 10.1016/j.rinp.2019.02.019.
[45] H. M. Kamari, N. M. Al-Hada, A. A. Baqer, A. H. Shaari, and E. Saion, "Comprehensive study on morphological, structural and optical properties of Cr_2O_3 nanoparticle and its antibacterial activities," *J. Mater. Sci., Mater. Electron.*, vol. 30, no. 8, pp. 8035–8046, Apr. 2019.
[46] N. Al-Hada, H. Kamari, A. Baqer, A. Shaari, and E. Saion, "Thermal calcination-based production of SnO_2 nanopowder: An analysis of SnO_2 nanoparticle characteristics and antibacterial activities," *Nanomaterials*, vol. 8, no. 4, p. 250, 2018.
[47] B. Cullity, *Elements of X-ray Diffraction*, 2nd ed. Reading, MA, USA: Addison-Wesley, 1978.
[48] K. Anandan and V. Rajendran, "Size controlled synthesis of SnO_2 nanoparticles: Facile solvothermal process," *J. Non-Oxide Glasses*, vol. 2, no. 2, pp. 83–89, 2010.
[49] A. A. Firooz, A. R. Mahjoub, and A. A. Khodadadi, "Preparation of SnO_2 nanoparticles and nanorods by using a hydrothermal method at low temperature," *Mater. Lett.*, vol. 62, nos. 12–13, pp. 1789–1792, Apr. 2008, doi: 10.1016/j.matlet.2007.10.004.
[50] H. Kamari, N. Al-Hada, E. Saion, A. Shaari, Z. Talib, M. Flaifel, and A. Ahmed, "Calcined solution-based PVP influence on ZnO semiconductor nanoparticle properties," *Crystals*, vol. 7, no. 2, p. 2, 2017.
[51] A. Salem, E. Saion, N. M. Al-Hada, H. M. Kamari, A. H. Shaari, and S. Radiman, "Simple synthesis of ZnSe nanoparticles by thermal treatment and their characterization," *Results Phys.*, vol. 7, pp. 1175–1180, 2017.
[52] A. A. Baqer, K. A. Matori, N. M. Al-Hada, A. H. Shaari, E. Saion, and J. L. Y. Chyi, "Synthesis, structural and optical properties of cerium oxide nanoparticles prepared by thermal treatment method," *Solid State Phenomena*, vol. 268, pp. 132–137, Oct. 2017.
[53] N. Al-Hada, E. Saion, Z. Talib, and A. Shaari, "The impact of polyvinylpyrrolidone on properties of cadmium oxide semiconductor nanoparticles manufactured by heat treatment technique," *Polymers*, vol. 8, no. 4, p. 113, 2016.
[54] A. A. Baqer, K. A. Matori, N. M. Al-Hada, A. H. Shaari, H. M. Kamari, E. Saion, J. L. Y. Chyi, and C. A. C. Abdullah, "Synthesis and characterization of binary $(CuO)_{0.6}(CeO_2)_{0.4}$ nanoparticles via a simple heat treatment method," *Results Phys.*, vol. 9, pp. 471–478, Jun. 2018.
[55] N. M. Al-Hada, H. Mohamed Kamari, C. A. C. Abdullah, E. Saion, A. H. Shaari, Z. A. Talib, and K. Matori, "Down-top nanofabrication of binary $(CdO)_x(ZnO)_{1-x}$ nanoparticles and their antibacterial activity," *Int. J. Nanomed.*, vol. 12, pp. 8309–8323, Nov. 2017.
[56] A. A. Baqer, K. A. Matori, N. M. Al-Hada, H. M. Kamari, A. H. Shaari, E. Saion, and J. L. Y. Chyi, "Copper oxide nanoparticles synthesized by a heat treatment approach with structural, morphological and optical characteristics," *J. Mater. Sci., Mater. Electron.*, vol. 29, no. 2, pp. 1025–1033, 2017.
[57] N. M. Al-Hada, E. Saion, H. M. Kamari, M. H. Flaifel, A. H. Shaari, Z. A. Talib, N. Abdullahi, A. A. Baqer, and A. Kharazmi, "Structural, morphological and optical behaviour of PVP capped binary $(ZnO)_{0.4}(CdO)_{0.6}$ nanoparticles synthesised by a facile thermal route," *Mater. Sci. Semicond. Process.*, vol. 53, pp. 56–65, Oct. 2016.
[58] L. B. Zakiyah, E. Saion, N. M. Al-Hada, E. Gharibshahi, A. Salem, N. Soltani, and S. Gene, "Up-scalable synthesis of size-controlled copper ferrite nanocrystals by thermal treatment method," *Mater. Sci. Semicond. Process.*, vol. 40, pp. 564–569, Dec. 2015.
[59] E. J. Johnson, "Absorption near the fundamental edge," *Semiconductors Semimetals*, vol. 3, pp. 153–258, Jan. 1967.
[60] J. Torrent and V. Barron, *Encyclopedia of Surface And Colloid Science*. New York, NY, USA: Marcel Dekker, 2002, pp. 1438–1446.
[61] J. I. Pankove, *Optical Processes in Semiconductors*. New York, NY, USA: Dover, 2012.
[62] C. R. Aita, Y.-L. Liu, M. L. Kao, and S. D. Hansen, "Optical behavior of sputter-deposited vanadium pentoxide," *J. Appl. Phys.*, vol. 60, no. 2, pp. 749–753, Jul. 1986.
[63] S. Gnanam and V. Rajendran, "Luminescence properties of EG-assisted SnO_2 nanoparticles by sol-gel process," *Dig. J. Nanomater. Biostruct.*, vol. 5, no. 3, pp. 699–704, 2010.

[64] X. Xiang, X. T. Zu, S. Zhu, L. M. Wang, V. Shutthanandan, P. Nachimuthu, and Y. Zhang, "Photoluminescence of SnO_2 nanoparticles embedded in Al_2O_3," *J. Phys. D, Appl. Phys.*, vol. 41, no. 22, 2008, Art. no. 225102.

[65] F. Li, J. Song, H. Yang, S. Gan, Q. Zhang, D. Han, A. Ivaska, and L. Niu, "One-step synthesis of graphene/SnO_2 nanocomposites and its application in electrochemical supercapacitors," *Nanotechnol.*, vol. 20, no. 45, 2009, Art. no. 455602.

[66] T. Moon, S.-T. Hwang, D.-R. Jung, D. Son, C. Kim, J. Kim, M. Kang, and B. Park, "Hydroxyl-quenching effects on the photoluminescence properties of SnO_2:Eu^{3+} nanoparticles," *J. Phys. Chem. C*, vol. 111, no. 11, pp. 4164–4167, Mar. 2007.

[67] Z. Wang, H. A. Al-Jawhari, P. K. Nayak, J. A. Caraveo-Frescas, N. Wei, M. N. Hedhili, and H. N. Alshareef, "Low temperature processed complementary metal oxide semiconductor (CMOS) device by oxidation effect from capping layer," *Sci. Rep.*, vol. 5, no. 1, p. 9617, Sep. 2015.

[68] S. Stankovich, R. D. Piner, X. Chen, N. Wu, S. T. Nguyen, and R. S. Ruoff, "Stable aqueous dispersions of graphitic nanoplatelets via the reduction of exfoliated graphite oxide in the presence of poly(sodium 4-styrenesulfonate)," *J. Mater. Chem.*, vol. 16, no. 2, pp. 155–158, 2006.

[69] S. Das, D.-Y. Kim, C.-M. Choi, and Y. B. Hahn, "Structural evolution of SnO_2 nanostructure from core–shell faceted pyramids to nanorods and its gas-sensing properties," *J. Cryst. Growth*, vol. 314, no. 1, pp. 171–179, Jan. 2011, doi: 10.1016/j.jcrysgro.2010.10.151.

NAIF MOHAMMED AL-HADA received the B.Sc. degree in physics from Thamar University, Yemen, in 2002, and the M.Sc. degree in applied radiation physics and the Ph.D. degree in nanoscience and nanotechnology from Universiti Putra Malaysia (UPM), in 2011 and 2015, respectively.

From 2015 to 2019, he was appointed as a Postdoctoral Researcher with the Department of Physics, UPM. From June 2019 to October 2019, he was a Visiting Researcher with Universiti Teknologi Malaysia (UTM), Malaysia. Since October 2019, he has been a Lecturer with the Shandong Key Laboratory of Biophysics, Dezhou University (DZU), China. His research interests include nanoparticles synthesis and applications, metallic oxides nanostructures and its antibacterial activity, binary oxide nanostructures for solar cell and sensor applications, renewable energy, polymer composites/nanocomposites, conducting polymer nanocomposites, semiconductor nanotechnology, and applied radiation.

ABBAS M. AL-GHAILI received the B.Eng. degree (Hons.) in computer engineering from the University of Science and Technology, Sana'a, Yemen, in 2005, and the M. Sc. and Ph.D. degrees in computer systems engineering from Universiti Putra Malaysia (UPM), Serdang, Malaysia, in 2009 and 2013, respectively.

Since February 2018, he has been a Postdoctoral Researcher with the Institute of Informatics and Computing in Energy (IICE), Universiti Tenaga Nasional (UNITEN), Malaysia. His research interests include image processing, artificial intelligence, and energy informatics.

Dr. Al-Ghaili is a member of the International Association of Computer Science and Information Technology and the Universal Association of Computer and Electronics Engineers.

HAIROLADENAN KASIM is currently a Senior Lecturer with the College of Computing and Informatics (CCI), UNITEN, Kajang, Malaysia. His research interests include energy informatics and energy and computing.

MUNEER AZIZ SALEH received the B.Sc. degree in physics from Sanaá University, Yemen, the M.Sc. degree in applied physics from the National University of Malaysia, Malaysia, and the Ph.D. degree from University Technology Malaysia (UTM), in January 2014. He is currently a Lecturer with the Nuclear Engineering Program, Faculty of Chemical and Energy Engineering, UTM. His research interests include environmental radiology, radiation dosimetry, nuclear powerplant siting, radiation protection, and reactor physics.

MOAYAD HUSEIN FLAIFEL received the B.Sc. (Hons.) and M.Sc. (Hons.) degrees in physics form Aligarh Muslim University, India, in 2001 and 2003, respectively, and the Ph.D. degree in materials science with specialization in composites and nanomaterials from the National University of Malaysia (UKM), Malaysia, in 2012.

He is currently an Assistant Professor with the Department of Physics, College of Science, Imam Abdulrahman Bin Faisal University, Saudi Arabia. He has taught several courses in materials science and engineering and physics for both undergraduate and postgraduate level. His research interests include polymer composites/nanocomposites, nanoparticles, nanomaterials, thin film nanotechnology, microwave absorption application, and electronic packaging application.

HALIMAH MOHAMED KAMARI is currently a Lecturer with Universiti Putra Malaysia, Malaysia. Her research interests include material characterization materials, nanomaterials, optoelectronics, heat treatment, microstructure, glasses, thin films, and nanotechnology.

HUSSEIN BAQIAH received the Master of Science degree from Putra University Malaysia, in 2009, and the Ph.D. degree in materials science from the National University of Malaysia (UKM), in 2014.

From 2015 to 2019, he worked as a Postdoctoral Researcher with Putra University Malaysia. Since October 2019, he has been a Lecturer with the Shandong Key Laboratory of Biophysics, Dezhou University (DZU), China. His research interests are in synthesis and explore physical properties (structural, electrical, optical, magnetic, and electronic) of multifunctional thin films, nanocomposites, bulk materials for optoelectronic, sensor, spintronics, and photoenergy conversion, and superconductors applications.

JIAN LIU received the B.S. degree in biotechnology from Yantai University, China, in 2003, the M.Sc. degree in genetics from Nanjing Agriculture University, China, in 2007, and the Ph.D. degree in microbial and enzymatic engineering from INSA-Toulouse, France, in 2015.

From 2015 to 2017, he was appointed as a Postdoctoral Researcher at Toulouse White Biotechnology, France. Since June 2018, he has been a Lecturer with the Shandong Key Laboratory of Biophysics, Dezhou University (DZU), China. His research interests include microbiology, microbiome, plant disease, and biotechnology.

WANG JIHUA is currently the Director of the Institute of Biophysics, Dezhou University, China. He is also a Ph.D. Tutor with Shandong Normal University. He is a council member of the Chinese Biophysics Society. He obtained the Special Allowance of the State Council and is nominated as Scientists with Outstanding Contribution of Shandong. He has undertaken more than ten scientific research funds, including funds from the National Science Foundation of China. He has published more than seventy articles in well-known journals such as Nuclei Acids Research, Nature Communications, Biophysical Journal, Physics Review, Journal of Theoretical Biology, and Biophysics journal. He has received five national patents. His research interests include long non-coding RNAs, intrinsically disordered proteins and modern biophysical cross-discipline technologies.